Condensin-driven loop extrusion on supercoiled DNA

Kim, Eugene; Gonzalez, Alejandro Martin; Pradhan, Biswajit; van der Torre, Jaco; Dekker, Cees

Important note
To cite this publication, please use the final published version (if applicable).
Please check the document version above.

Check for updates

Condensin-driven loop extrusion on supercoiled DNA

Eugene Kim[1,2], Alejandro Martin Gonzalez [1], Biswajit Pradhan[1,2], Jaco van der Torre[1] and Cees Dekker [1✉]

Condensin, a structural maintenance of chromosomes (SMC) complex, has been shown to be a molecular motor protein that organizes chromosomes by extruding loops of DNA. In cells, such loop extrusion is challenged by many potential conflicts, for example, the torsional stresses that are generated by other DNA-processing enzymes. It has so far remained unclear how DNA supercoiling affects loop extrusion. Here, we use time-lapse single-molecule imaging to study condensin-driven DNA loop extrusion on supercoiled DNA. We find that condensin binding and DNA looping are stimulated by positively supercoiled DNA, and condensin preferentially binds near the tips of supercoiled plectonemes. Upon loop extrusion, condensin collects nearby plectonemes into a single supercoiled loop that is highly stable. Atomic force microscopy imaging shows that condensin generates supercoils in the presence of ATP. Our findings provide insight into the topology-regulated loading and formation of supercoiled loops by SMC complexes and clarify the interplay of loop extrusion and supercoiling.

SMC complexes such as condensin and cohesin are key players for DNA organization in all organisms[1]. These SMCs organize chromosomes into loops as a result of DNA loop extrusion, a hypothesis that was directly confirmed by recent single-molecule experiments[2–6]. However, these in vitro studies typically used a straight piece of naked DNA, whereas DNA in cells is supercoiled, entangled and bound by a myriad of DNA-binding proteins. Torsional stresses, which are inevitably induced by transcription and replication fork progression, cause DNA to adopt superhelical structures with locally underwound or overwound DNA, known as negative or positive supercoiling, respectively. Such supercoiling typically involves large structural rearrangements of the DNA through the formation of plectonemes in which the DNA helix is coiled onto itself (Fig. 1a). It remains unknown how the loop-extrusion activity of SMC proteins deals with the supercoiling states of DNA that are abundant in cells.

Previous reports pointed to various DNA-supercoiling-specific interactions of SMC complexes. In yeast, mitotic DNA was found to manifest positive supercoiling that was dependent on the SMC2 subunit of condensin[7], condensin was suggested to reduce transcription-induced underwound DNA[8], and chromatin immunoprecipitation and sequencing (ChIP-seq) data suggested that cohesin can trap torsional stresses ahead of the replication fork[9]. In mammalian cells, it was shown that cohesin-mediated DNA loops induce topological stresses[10]. Gel-based[11,12] and electron-imaging[13] studies of condensin I from *Xenopus* egg extract showed an ATP-dependent generation of supercoiling in plasmids, and human condensin I showed similar results[14]. Other in vitro studies showed that yeast condensin[15] and Smc5/6[16] can stabilize plectonemes on supercoiled DNA, whereas the cohesin heterodimer Smc1/3 was reported to compact DNA in a supercoiling-dependent fashion[17]. Despite all these data, mechanistic insights are largely lacking, and it remains unclear how these findings are linked to the recently found DNA-loop-extrusion activity of SMC proteins.

Here, we use real-time single-molecule imaging to study the dynamic interplay of DNA supercoiling and DNA loop extrusion

by yeast condensin. We find that DNA binding and loop extrusion by condensin are stimulated by positive supercoiling. Condensin is found to preferentially bind to the tip of plectonemes, whereupon it starts loop extrusion. Surprisingly, we find that loop extrusion by condensin absorbs all plectonemes on supercoiled DNA and locks them into a single supercoiled loop that is highly stable. The resulting supercoiled DNA loop subsequently acts as a favorable substrate for recruiting additional condensins. Atomic force microscopy (AFM) imaging shows that condensin generates DNA supercoiling in an ATP-dependent manner. Finally, we discuss how our in vitro observations of the strong effect of DNA supercoiling on loop extrusion mechanics may impact DNA loop extrusion in cells.

Results

Loop-extruding condensin absorbs nearby plectonemes into one supercoiled loop. To study the interaction between condensin and supercoiled DNA, we generated positively supercoiled DNA by adding intercalating SYTOX Orange (SxO) dyes onto torsionally constrained 42-kilobase (kb) DNA substrates that were attached to a passivated surface at both ends with multiple binding groups[18,19] (Fig. 1a). Visualization was done using highly inclined and laminated optical sheet (HILO) microscopy. Similarly, negatively supercoiled DNA could be made by attaching pre-SxO-loaded DNA to the surface and subsequently reducing the SxO concentration[18]. The handedness of generated DNA supercoiling was confirmed by control experiments using *Escherichia coli* topoisomerase I, which selectively relaxes negative supercoils only (Extended Data Fig. 1). All experiments were done on positively supercoiled DNA unless denoted otherwise.

Individual plectonemes were directly observable as local intensity maxima along the DNA, and their position, intensity and number dynamically changed over time very frequently, consistent with findings from previous reports[18–20]. Stretching these DNA spots sideways by applying buffer flow perpendicular to the attached DNA showed elongated DNA structures with a higher intensity than the rest of the DNA tether, indicating a plectoneme with two DNA
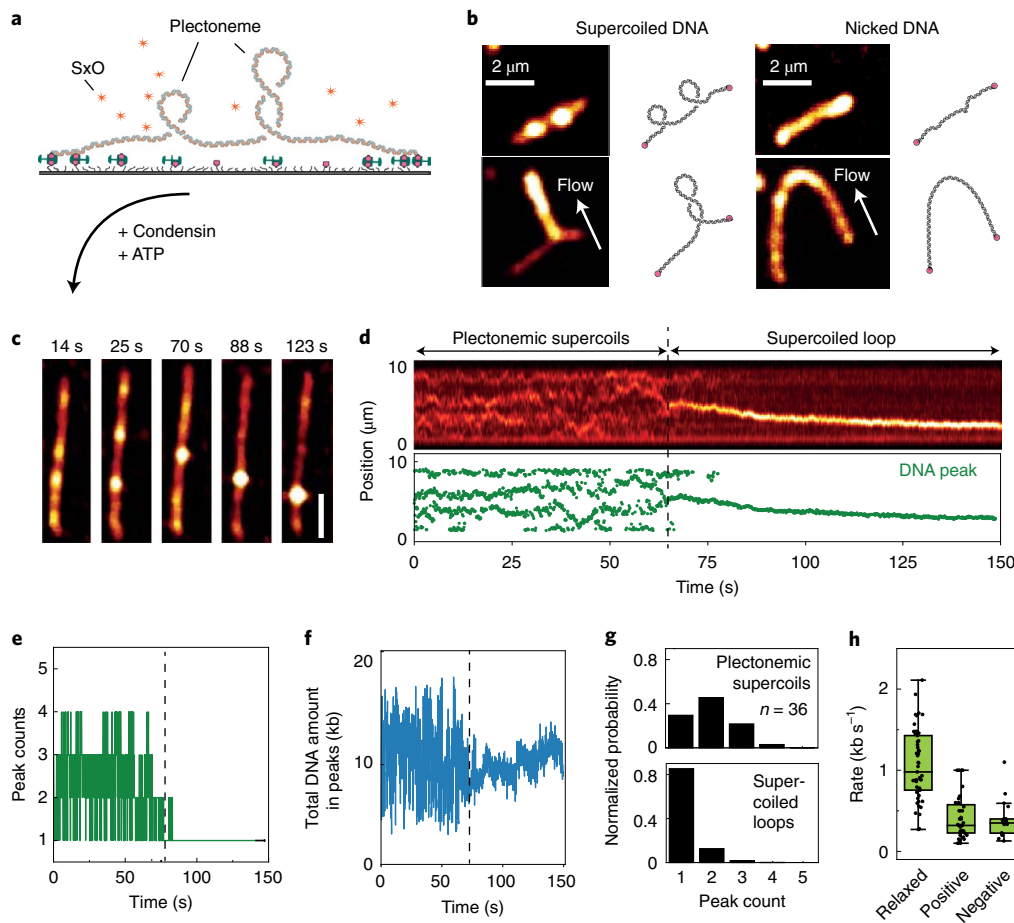
Fig. 1 | Condensin-mediated loop extrusion collects and stabilizes plectonemes into a single supercoiled DNA loop. a, Schematic of intercalation-induced DNA supercoiling assay used for this study. **b**, Snapshots showing single-molecule visualizations of double-tethered, SxO-stained supercoiled DNA (left) containing multiple plectonemes (top left) that can be stretched into a single plectoneme (bottom left), and the images of the same nonsupercoiled molecule after nicking (right). Arrows indicate the direction of buffer flow. Data represent four independent experiments. **c,d**, Snapshots (**c**), fluorescence-intensity kymograph (**d**, top) and the corresponding individual DNA peak positions (**d**, bottom), showing a loop extrusion event on supercoiled DNA. Scale bar in **c** indicates 2 μm. **e**, Corresponding number of total DNA peaks in **d**. **f**, The total amount of DNA within the DNA peaks in **c** and **d** versus time. Data in **c–f** represent 11 independent experiments. **g**, Comparison of the number of DNA peaks before (top) and after (bottom) the loop extrusion from n = 36 molecules. **h**, Rate of loop extrusion for relaxed DNA, positively supercoiled DNA and negatively supercoiled DNA, from n = 49, 36 and 17 molecules, respectively. The box plots span from the 25th to 75th percentiles, the center line shows the median and whiskers show maximum and minimum values. P value is 1.5×10^{-10}; two-sided t-test.

helices that were mutually intertwined (Fig. 1b). Unlike the open loops that we observed for nicked DNA[2], we did not observe any temporary separation of the two arms, consistent with the plectonemic DNA structure. Upon nicking the same molecule with a prolonged exposure of excitation light, the plectonemes abruptly disappeared, the DNA image changed to exhibit a homogenous intensity, and side flow stretched the DNA into an arc shape, all confirming that the DNA relaxed to a torsionally unconstrained state upon nicking.

Upon the addition of condensin (1–2 nM) in the presence of ATP (5 mM) to supercoiled DNA, the dynamic plectonemic state changed into a single spot that grew in intensity over time (Fig. 1c,d). More specifically, at time $t \sim 67$ s in Fig. 1d, a single DNA intensity peak appeared among the multiple plectoneme peaks and gradually increased in size as it moved along the DNA, until it stalled ($t \sim 120$ s). This observation is clearly reminiscent of the characteristic dynamics of condensin-mediated loop extrusion. Strikingly, however, for this supercoiled DNA, all of the plectonemes that were continuously present at $t < 67$ s disappeared upon the onset of the condensin-mediated DNA loop extrusion, whereupon all DNA

intensity was concentrated at the loop location ($t \sim 77$ s, Fig. 1d; see Extended Data Fig. 2 and Supplementary Video 1 for more examples). Figure 1e quantifies our observation and shows that one to four plectonemes (mean, 2.6) were present before $t = 67$ s, whereas a single peak was observed after the loop extrusion ($t \sim 77$ s). The final amount of DNA that was collected to the loop location was not much larger than the amount of DNA within the plectonemes that were initially present (Fig. 1f), indicating that condensin gathered the plectonemic DNA during loop extrusion but not substantially more. These data indicate that upon the formation of a loop, condensin collects the plectonemes along the 42-kb DNA and stabilizes them at its location.

The behavior that condensin-driven DNA loop extrusion leads to an abrupt transition from a dynamic plectonemic state to a stable loop by the collection of plectonemes into a single position was consistently observed in nearly all loop extrusion events that we analyzed (n = 32 out of 36, Fig. 1g). There were a few exceptions in which one or more plectonemes remained after loop formation (Extended Data Fig. 2). Note that in the latter cases, condensin was bound near the tethered end of DNA and the (asymmetric)
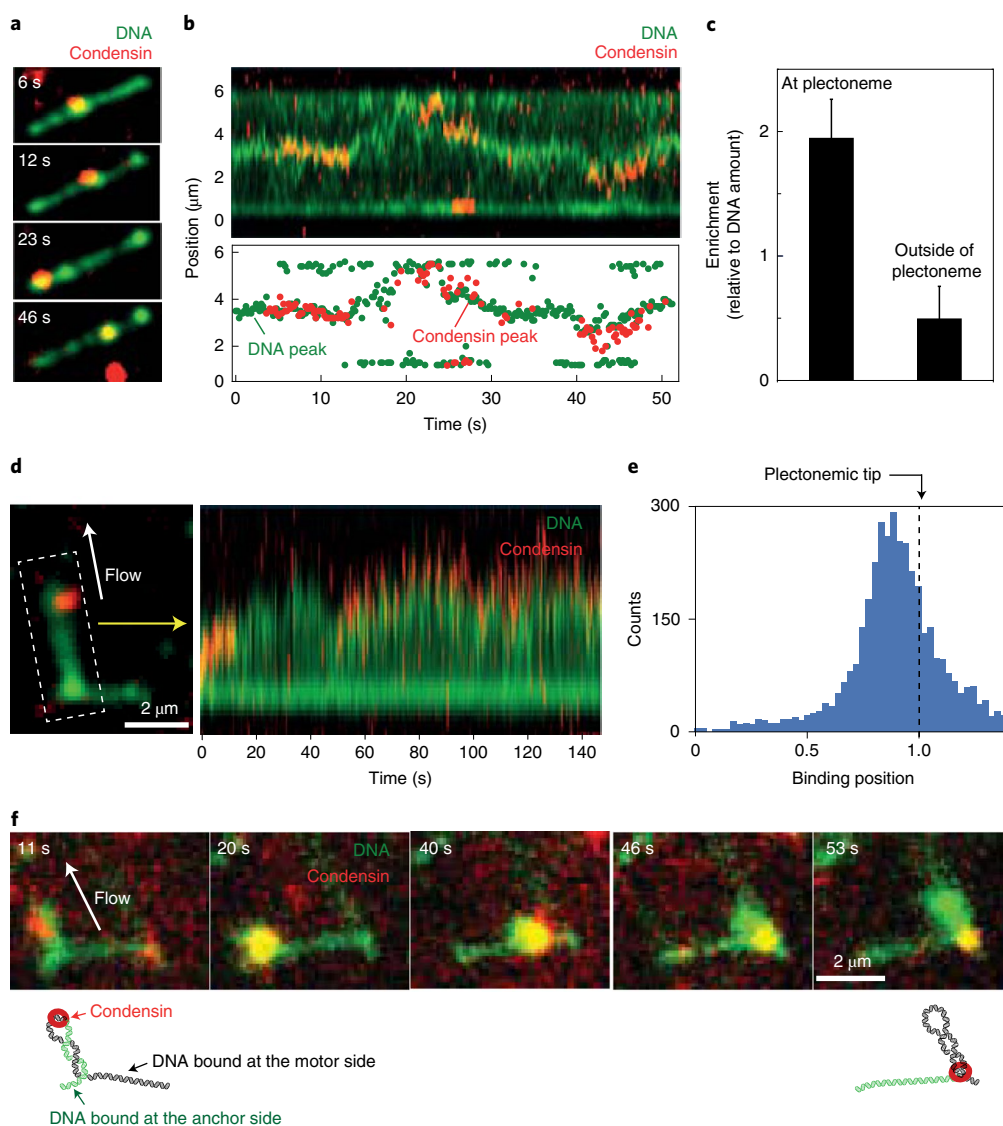
Fig. 2 | Condensin loads near a plectoneme tip and moves downward along the plectoneme upon loop extrusion. a,b, Snapshots (**a**), a kymograph (**b**, top) and the associated positions of SxO-stained DNA and Atto 647N-labeled condensin peaks (**b**, bottom), showing co-localizations of condensins and DNA plectonemes. Data in **a** and **b** represent eight independent experiments. **c,** Enrichment of condensin at DNA plectonemes relative to the amount of DNA outside plectonemes. Data shows the mean ± 95% confidence interval ($n = 49$ molecules). **d,** Snapshot (left) and kymograph (right) showing condensin localization near the plectoneme tip. The dashed box indicates the area of the image included to build the kymograph (right), as indicated with a yellow arrow. Data represent three independent experiments. **e,** Binding distribution of condensin along the length of DNA plectonemes estimated from the kymographs as in **d** for $n = 27$ molecules, where the scale 0–1 denotes the position from the stem to the tip along the plectoneme. **f,** Snapshots (top) showing condensin moving from the plectoneme tip (11 s) toward the stem (>20 s). Simultaneously, the plectoneme becomes compacted (20 s) and moves together with condensin during extrusion, while it grows back its length (40–53 s). Data represent three independent experiments. Schematics (bottom) show the corresponding molecular pictures of asymmetric loop extrusion by condensin on supercoiled DNA.

DNA loop extrusion was limited by reaching the end position of the DNA. Given that the linking number (a measure of the degree of supercoiling writhe) is conserved in a topologically constrained DNA molecule, the vanishing of plectonemes along the two arms of the DNA molecule indicates that the local region of the extruded loop should be highly supercoiled.

We compared the speed of DNA loop extrusion between supercoiled and relaxed DNA (Fig. 1h), as obtained from the slope of the initial linear part of the loop growth versus time (cf. Fig. 1d between 69 s and 89 s). The observed mean rate (Fig. 1h) for supercoiled DNA (~0.4 kb s⁻¹; for both positive and negative supercoiling) was almost a factor three lower than that of torsionally relaxed DNA (~1.1 kb s⁻¹). This may indicate that the resulting supercoiled

topology of the DNA loop that is being extruded slows down the speed of loop extrusion.

Condensin loads near a plectoneme tip upon loop extrusion. Where does condensin bind to supercoiled DNA, and how does it relocate upon loop extrusion? To address these questions, we co-imaged DNA with condensin complexes that were labeled with a single fluorophore (Atto 647N). Interestingly, we observed that condensin often bound at a plectoneme, then diffused together with it along the DNA, whereupon it unbound without extruding a DNA loop (Fig. 2a,b). We found that about 30% of all binding events led to loop extrusion, while the rest led to unbinding events ($n = 41$). Such temporary binding events of condensin, which did not induce
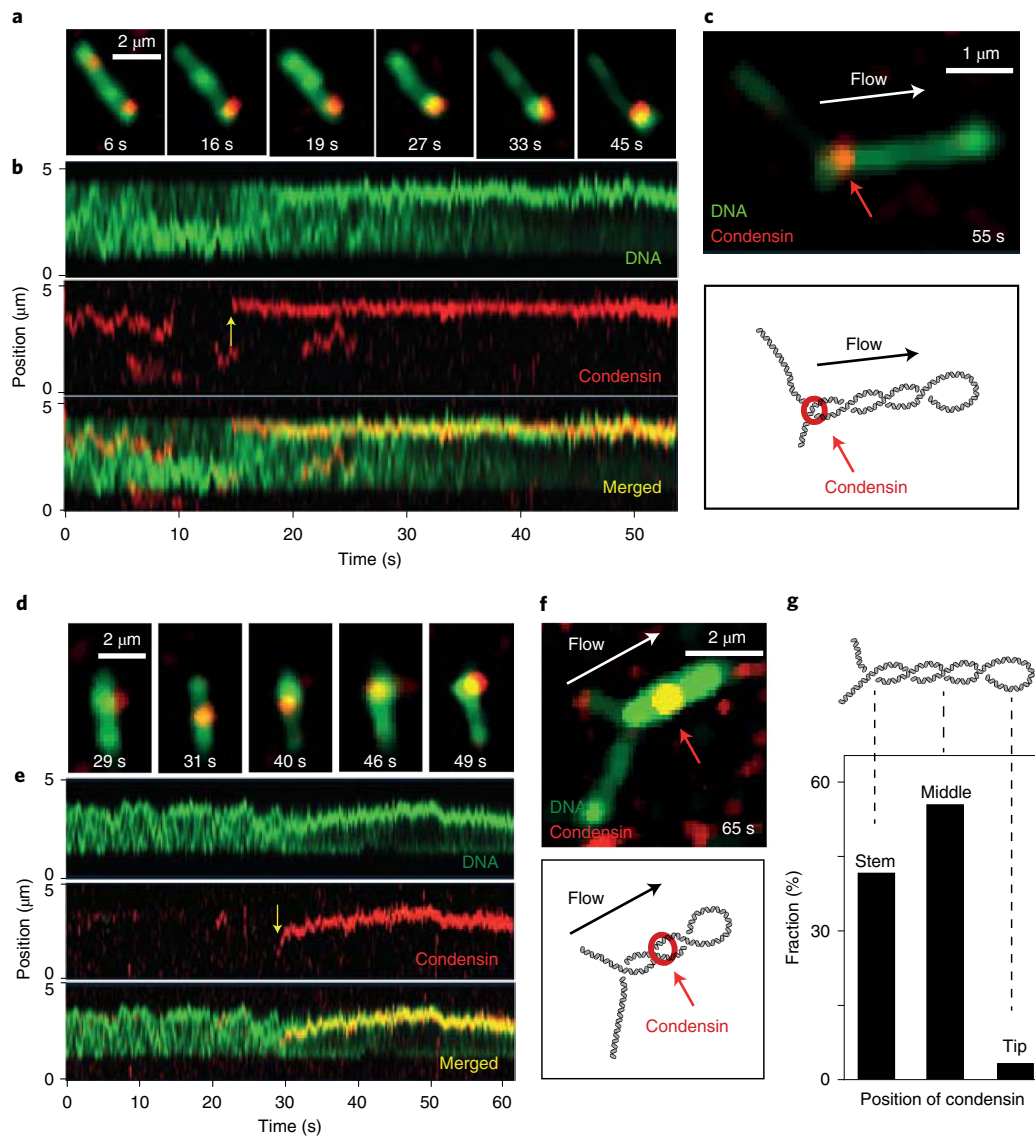
Fig. 3 | Condensin is located at the stem or at the middle of a plectoneme after extrusion of a supercoiled loop. a,b, Snapshots (**a**) and kymographs (**b**) showing loop extrusion on supercoiled DNA. The yellow arrow in **b** indicates the binding of condensin that subsequently led to loop extrusion. **c**, Snapshot (top) and schematic (bottom) of a molecule in **a** and **b** in side flow, revealing the location of condensin along the plectoneme at the stem after extrusion of the supercoiled loop. **d**–**f**, Snapshots (**d**), kymographs (**e**) and the resulting snapshot with side flow (**f**) of the supercoiled loop extrusion event, which shows a condensin located at the middle of a plectoneme after extrusion. Data in **a**–**f** represent five independent experiments. **g**, Fractions of occurrence of different condensin positions after extrusion of supercoiled DNA ($n = 36$ molecules).

loop extrusion, were also reported for nonsupercoiled DNA[21]. The enrichment of condensins at plectonemes, estimated by normalizing the co-localization probability of condensin and plectoneme peaks with the average amount of DNA inside plectonemes (Fig. 2b; see Methods), revealed that condensins were four times more likely to be observed at plectonemes than outside of plectonemes ($n = 49$; Fig. 2c). This shows that condensin has a higher binding affinity to plectonemic supercoiled DNA than to regular nonplectonemic DNA.

Subsequently, we determined the preferred binding location of condensin within a plectoneme (stem, middle or tip). To this end, we quantified the binding locations of condensin complexes on side-flow-stretched plectonemes (Fig. 2d). Kymographs plotted along the length of a stretched DNA plectoneme clearly showed that the majority of condensins initially bound near the plectoneme tip (Fig. 2d). Quantification of the binding events ($n = 27$ molecules; Fig. 2e) showed a peak at a position of ~0.9, where a value 0

corresponds to the plectoneme stem and 1 corresponds to the tip, indicating that the majority of condensins bound in the vicinity of the plectoneme tip. This suggests that condensin favors binding at the apical loops of the DNA plectoneme tip, instead of at DNA crossings at the plectoneme body or at the stem. This is further supported by the AFM data, which showed that condensin binding was enriched near the apices of plectonemes (Extended Data Fig. 3). Upon loop extrusion, the plectoneme-tip-bound condensins moved downward, ending up in the middle or bottom of the plectoneme (11 s, Fig. 2f; see Extended Data Fig. 4 for more examples), as manifested by the changes of condensin position within the flow-directed plectonemes. Upon reaching the bottom of the plectoneme, the plectoneme shrunk in size (20 s), whereupon it gradually regained its larger size while moving together with condensin (20–53 s). As budding yeast condensin also extrudes the DNA loop asymmetrically[2] on supercoiled DNA (Extended Data Fig. 5), we
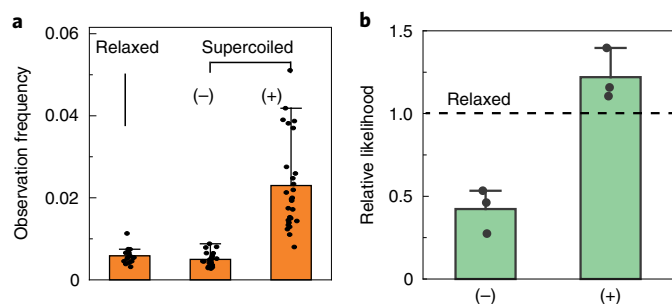
Fig. 4 | Positive supercoiling promotes condensin loading and loop formation, whereas negative supercoiling does not. a, Probability of observing a condensin holocomplex on relaxed (nicked), negatively supercoiled (−) and positively supercoiled (+) DNA. Numbers are calibrated as observation frequency per 1 kb of DNA length ($n = 17$, 26 and 31 for relaxed, negatively coiled and positively coiled substrates, respectively). **b**, Probability of observing loops on negatively and positively coiled substrates relative to relaxed (nicked) DNA, compared under the same conditions (in a steady-state regime after adding condensin and ATP for 10 min) in the same field of view. Data represent mean ± s.d. Error bars in **a** show the s.d. of the measured individual values. Error bars in **b** show the s.d. from averaging the three independent experiments.

interpret these observations as follows. When a one-sided motor condensin binds near the tip of a plectoneme and extrudes a supercoiled loop, it absorbs the DNA connected to the 'motor side' of the condensin into the loop, thereby moving downward and further compacting the plectoneme. When condensin reaches the stem of the plectoneme, it continues to reel in more DNA in the arm connected to the motor side of the DNA (black DNA in the schematics in Fig. 2f). This continued motor action will then move the position of the plectoneme loop, while simultaneously increasing the length of the extruded plectonemic loop (20–53 s). Meanwhile, the increasing tension within the DNA outside of the extruded loop results in further stretching of the DNA, both in the DNA arm on the motor side and in the DNA on the anchor side of condensin, resolving other plectonemes that previously resided there. This indicates that the disappearance of plectonemes from the anchor side and motor side of condensin should be attributed to different mechanisms. Whereas plectonemes at the motor side can be absorbed into the writhe of the supercoiled loop, the plectonemes connected to the anchor side disappear because of increased tension within the DNA. This is further supported by our data that quantify the amount of DNA on both sides of the extruding loop (Extended Data Fig. 6); although plectonemes disappear at both arms of condensin, only the amount of DNA connected to the motor side decreases, indicating that the absorption of plectonemes only occurs on the motor side.

Figure 3 visualizes condensin as it gets localized at the stem or at the middle of a plectoneme after extrusion of a supercoiled loop. In accordance with the observations in Figs. 1 and 2, condensin mostly bound to the tip of a plectoneme ($n = 25$ out of 30 molecules; for example, $t = 16$ s in Fig. 3a,b; Supplementary Video 2) and gradually reeled in DNA while simultaneously localizing all of the plectonemes near the condensin location (until $t \sim 40$ s, Fig. 3a,b). After the loop was formed, we applied a buffer flow ($t = 55$ s) and monitored the location of condensin along the supercoiled DNA loop (Fig. 3c; see Extended Data Fig. 7 for more examples). This revealed that condensin was localized at the stem of the plectonemic loop. We also observed condensins that extruded a supercoiled loop with similar dynamics (Fig. 3d,e), which ended up at a central location along the plectoneme (Fig. 3f; see Extended Data Fig. 7 for more examples). Even in these cases, all plectonemes in the DNA were

still localized into the position of the extruded loop ($t > 45$ s, Fig. 3e). The localization of condensin occurred with similar frequencies at the stem and in the central body of the supercoiled loop after extrusion, and condensins were rarely located near the tip after loop extrusion (Fig. 3g). These data suggest that the condensin-mediated supercoiled loop does adopt plectonemes from outside the loop region to incorporate them inside the extruded loop or to stabilize them to a position just below the condensin complex.

Positive supercoiling promotes condensin loading and loop extrusion. We further investigated whether the observed preferential loading of condensin on plectonemic DNA was dependent on the handedness of the DNA supercoiling. Interestingly, the probability to bind condensin to positively supercoiled DNA was found to be about fourfold higher than the probability to bind to relaxed DNA (Fig. 4a). Remarkably, the binding affinity of condensin to negatively supercoiled DNA was similar to that of relaxed DNA (Fig. 4a), which indicates that condensin clearly favors binding to an overwound plectonemic DNA topology (positive supercoiling).

We then questioned whether the strong dependence of the binding affinity of condensin on the chirality of supercoiling would also affect the consequent loop formation probability. For this, we measured the fraction of all double-tethered DNA molecules that displayed a loop, and we compared the results for positively supercoiled DNA with those for relaxed DNA in the same field of view, and similarly for negatively supercoiled DNA compared with relaxed DNA. Interestingly, the estimated looping probability for negatively supercoiled DNA was substantially lower (~0.32) than that for relaxed DNA, whereas it was higher for positive supercoils (~1.2, Fig. 4b). In other words, whereas positive supercoiling promotes DNA loop extrusion, negative supercoiling hinders it.

Condensin-driven loop extrusion generates DNA supercoiling. To visualize the condensin-mediated supercoiled loop with higher resolution, we used AFM and imaged the reaction products of condensin and topologically constrained DNA plasmids (2.96 kb in length) incubated with 1 mM of ATP, after drying the solution onto a mica substrate (see Methods). The plasmids were first nicked and re-ligated with T4 ligase to make them torsionally constrained circular double-stranded DNA (dsDNA) with zero additional linking number with respect to the relaxed (nicked) form. Indeed, as shown in Fig. 5a,b, this led to a majority of molecules (60%) that showed a circular DNA without any crossovers or other signatures of supercoiling. Single crossovers (that is, where a figure-zero plasmid was changed into a figure-eight shape) were also observed for these nonsupercoiled plasmids, which can be attributed to the deposition of the DNA onto the mica surface in AFM sample preparation[22]. Adding the condensin SMC complex in the absence of ATP did not lead to an increase in the number of crossovers in the plasmids.

However, when adding condensin with ATP, a dramatic change was observed and the large majority of plasmids (72%; $n = 128$) did get supercoiled, showing one or multiple crossovers (Fig. 5a,b). The majority of plasmids now consistently exhibited plectonemic conformations that appeared as high-intensity DNA lines consistent with two dsDNA molecules that are tightly wound around each other. Quantification of the images (Fig. 5b,c; see Methods and Extended Data Fig. 8 for the details of quantification methods) revealed that the initial plasmids showed only a ~30% fraction of entangled molecules (that is, with crossovers or plectonemic conformations; $n = 62$), whereas adding SMC and ATP shifted this distribution to a much larger fraction of >70% ($n = 109$). The data show that condensin can introduce a high degree of supercoiling into the plasmid DNA.

Next, we quantified the positions of condensins along the plasmids (Fig. 5d); we classified positions as outside the plectonemes, or at the stem, middle or tip of the plectonemes (see Fig. 5e for
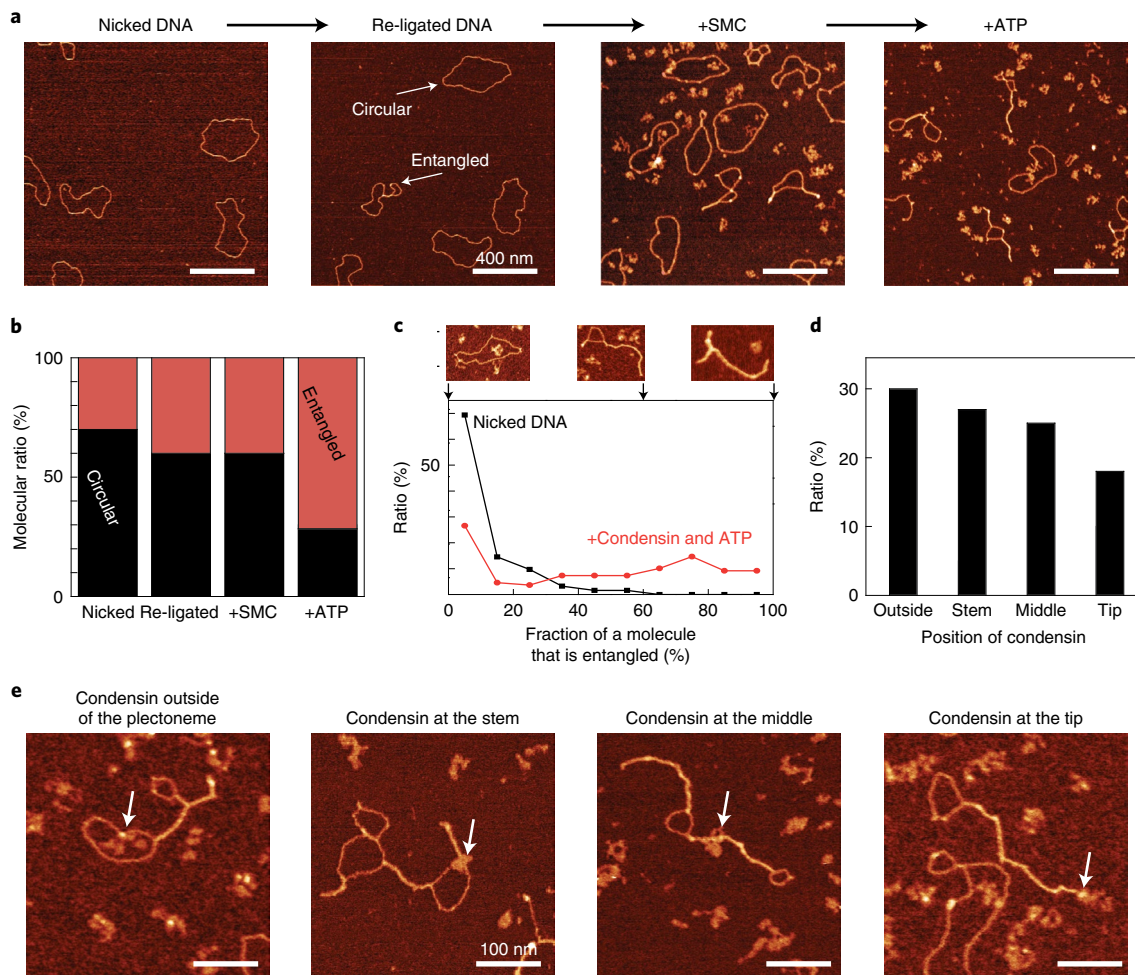
Fig. 5 | DNA supercoiling generation by condensin and ATP. a, Relaxed circular DNA molecules were nicked and re-ligated, and incubated with condensin and ATP. The presence of condensin and ATP increased the number of DNA molecules that exhibited supercoiling. **b**, Population graph of circular and entangled molecules for various conditions ($n = 102$, 128, 58 and 92 molecules, respectively). Data represent three independent experiments. **c**, Degree of entanglement for the nicked and condensin + ATP samples. Images on top show examples of DNA that was entangled to different degrees. **d**, Binding position of condensin bound to supercoiled DNA molecules. **e**, Examples of condensin bound to supercoiled DNA molecules. White arrows denote the position of the condensin complexes. Data represent three independent experiments.

examples). We found that, after the addition of condensin and ATP, condensin distributed rather equally among all four categories, with a slightly smaller fraction at the plectoneme tip.

Taken together, the AFM data show that the loop-extruding condensin complex introduces DNA supercoils into plasmid DNA by an ATP-driven process. In other words, the data show that condensin does not only passively absorb and trap existing plectonemes along DNA, as already indicated by our fluorescence-imaging data (Fig. 3), but it can also actively generate DNA supercoils.

Supercoiled DNA loops can recruit additional condensins. The preferential binding of condensin to DNA plectonemes (Fig. 2d) could lead to a situation in which multiple condensins bind to different plectonemes within the same DNA molecule. Interestingly, we observed that upon extrusion of a supercoiled loop, condensins that were bound at distant plectonemes could be jointly absorbed into one supercoiled loop. An example is presented in Fig. 6a,b, in which a condensin-driven supercoiled loop ($t > 16\,s$) approached ($t \sim 20\,s$) plectoneme-bound condensin(s) that were already present from $t < 16\,s$, to eventually merge into a single location ($t \sim 30\,s$). Subsequent imaging of the side-flow-stretched supercoiled loop after the merger (Fig. 6c; see Extended Data Fig. 7 for more

examples) clearly showed multiple condensins bound along the supercoiled loop.

Furthermore, we found that a supercoiled loop acts as a favorable substrate for the recruitment of additional condensins (Fig. 6d,e). Consistent with the findings in Fig. 2d, these additional condensins were often located near the tip of the supercoiled loops (Fig. 6f). Quantification of the locations of multiple condensins along supercoiled loops showed comparable numbers of condensins at the stem, in the middle and near the tip (Fig. 6g), a trend consistent with the findings from AFM imaging (Fig. 5d). We also estimated the number of condensins using photobleaching experiments at the supercoiled loop location in the absence of buffer flow (Extended Data Fig. 9). This showed that about 60% of all data (that is, combined with data shown in Fig. 3) involved a supercoiled DNA loop that contained a single condensin, whereas the remainder were composed of two or three condensins on the loop (Fig. 6h). We checked whether the recruitment of additional condensins on supercoiled loops was indeed attributed to the plectoneme structures, and not due to the relatively large amount of DNA within the extruded loop as compared with the outside of the loop. To this purpose, we compared the binding events of condensin molecules on relaxed DNA loops and on supercoiled
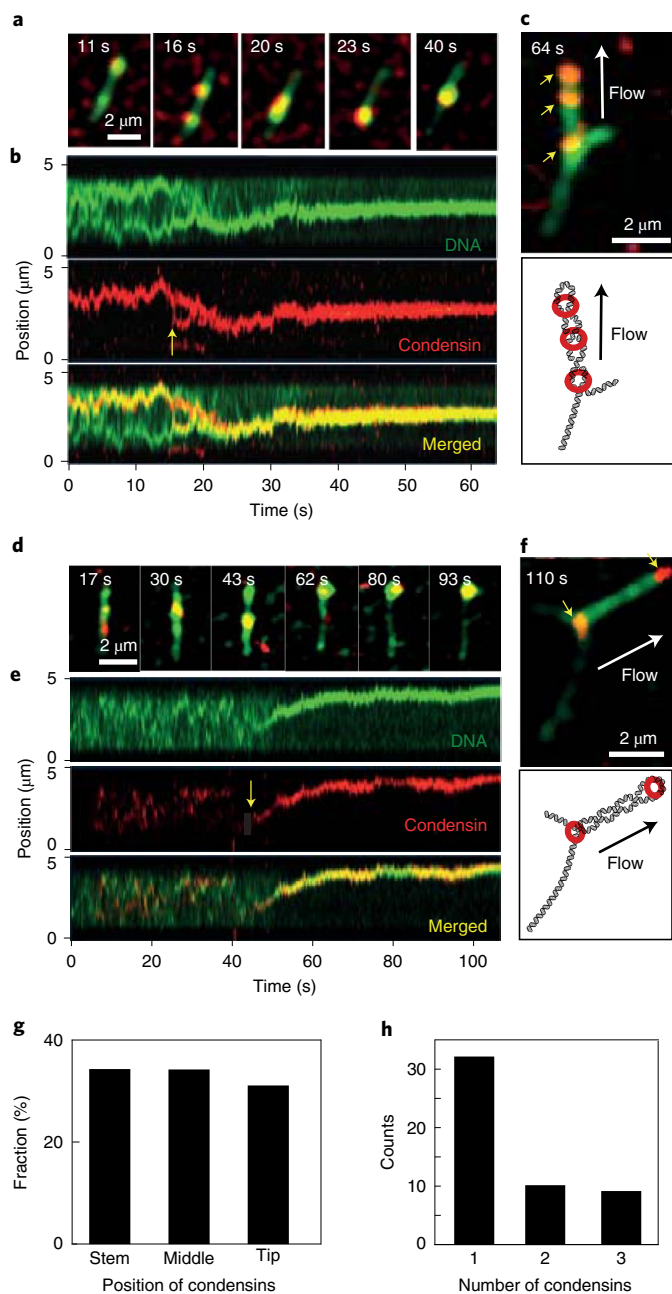
Fig. 6 | Recruitment of additional condensins onto a supercoiled loop.
a,b, Snapshots (**a**) and kymographs (**b**) showing the merging of multiple condensins by supercoiled loop extrusion. The yellow arrow in **b** indicates the binding position of a condensin that subsequently led to merging with another one(s). **c**, Snapshot under side flow (top) and schematic (bottom) of the molecule in **a** and **b**, revealing the location of multiple condensins along the plectoneme after the merger. **d–f**, Snapshots (**d**), kymographs (**e**) and the consequent snapshot under side flow (**f**) of the supercoiled loop, which shows an additional condensin bound on the tip of an extruded supercoiled loop. Yellow arrows in **c** and **f** indicate the locations of condensins. Data in **a–f** represent five independent experiments. **g**, Occurrence of different positions of condensins along the plectonemic loop after a supercoiled loop extrusion event for cases in which we observed multiple condensins ($n_{tot} = 61$ for 26 DNA molecules). **h**, Number of condensins on the supercoiled loop, estimated through photobleaching analyses.

DNA loops with similar lengths, which revealed a threefold higher binding rate onto plectonemic DNA (Extended Data Fig. 10). This indicates that the plectonemic structure of DNA supercoils

certainly promotes the additional binding of condensins onto supercoiled DNA loops.

Discussion

In this study, we used time-lapse single-molecule imaging and AFM to study condensin-mediated loop extrusion on supercoiled DNA. Whereas bacterial chromosomes exist in a globally negatively supercoiled form[23], eukaryotic chromosomes contain supercoiling domains of both positive and negative handedness, and both transcription and replication processes generate positive supercoiling ahead of the processing enzymes. Therefore, it is of general interest to examine how loop-extruding factors interact with these DNA topologies (both negative and positive handedness). Our findings provide a physical picture for the dynamic interplay of loop extrusion and DNA supercoiling (Fig. 7) as follows. Condensin initially binds at the tip of a supercoiled plectoneme (Fig. 7a,b) and starts reeling in the plectonemic DNA by loop extrusion. During loop growth, this emerging loop absorbs all of the neighboring plectonemes and puts them into one supercoiled loop that is highly stable (Fig. 7c,d). The motor action of condensin will bring the complex downward, where it ends up at a middle position along the body or it reaches the stem, and loop extrusion eventually stalls because of the stalling tension within the DNA[2]. The resulting supercoiled loop acts as a favorable substrate to further recruit additional condensins (Fig. 7e).

Surprisingly, our single-molecule imaging showed that condensin-induced loop extrusion clearly favors positively supercoiled DNA over negatively coiled DNA. Condensin loads with a higher affinity onto positively supercoiled DNA, and it extrudes DNA loops more frequently. Our data are consistent with early gel-based findings that condensin binds more abundantly to positively coiled plasmids[12]. These in vitro results suggest that in vivo condensin recruitment may be stimulated in regions where positive supercoils are generated, for example, ahead of transcription and replication machineries. This may explain the accumulation of condensins near transcription[8,24,25] and replication[26] sites. Topology-enhanced loading is likely a more general phenomenon among SMC proteins. For example, cohesin and SMC5/6 have also been found to co-localize within regions where higher levels of catenation and torsional stress are present[9,10,27,28].

Our flow-induced visualization assay further showed that condensin initially bound preferentially near the plectoneme tip (Fig. 2d,e). We speculate that this may be due to the well-defined apical teardrop-shape loop structure at the tip of plectoneme, which has a diameter of tens of nanometers[29], that may serve as a favorable substrate for condensin, as it allows binding at two positions within the protein complex. Furthermore, the highly curved plectoneme tip may help condensin to start loop extrusion by circumventing the high energy cost associated with bending DNA in the initiation of loop extrusion.

Surprisingly, we found that the loop extrusion activity of condensin led to the absorption of all nearby plectonemes (Figs. 1 and 3). In other words, loop extrusion removes all supercoiling writhe from DNA and locks that into one localized spot, thus profoundly changing the DNA topology. This occurred over the full range of our 42-kb DNA, which provides a lower bound estimate for the range of the region where plectonemes are collected, as this length is limited in our assay. Our observation that loop extrusion incorporates existing intertwined structures does not support earlier ideas that an SMC loop extruder would act as a topological roadblock that would accumulate topological stresses ahead of the motor[10], or that supercoiling itself can push SMCs[30]. The finding that loop extrusion localizes plectonemic supercoils in one defined location at the SMC may have interesting in vivo implications. It is tempting to speculate that the supercoiling domains found in cells[28,31,32] may be organized by the plectoneme-localizing activity of SMCs. Interestingly, the mean size of supercoiling domains (~100 kb) found in human
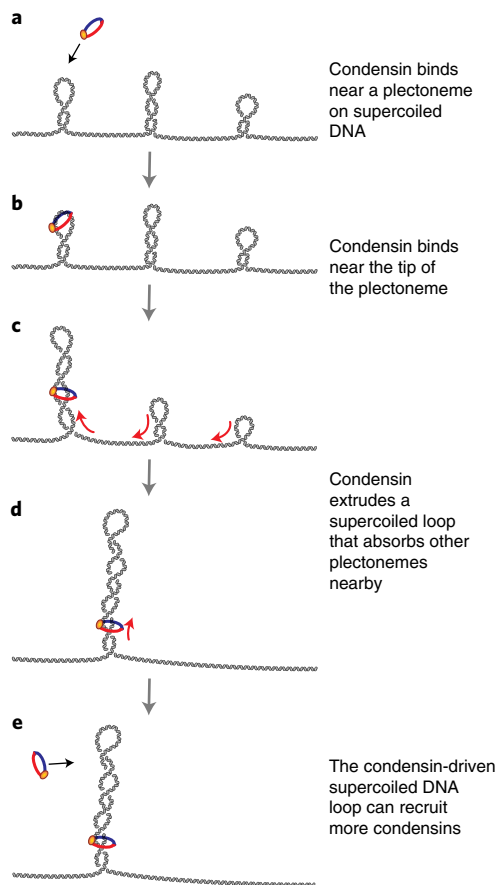
Fig. 7 | Model for condensin-mediated loop extrusion on supercoiled DNA. a–e, A condensin SMC complex loads at a DNA plectoneme (**a**), near its tip (**b**), and subsequently initiates the extrusion of a DNA loop that absorbs all neighboring plectonemes and locks them into a single supercoiled loop (**c**,**d**), which can be followed by the recruitment of additional condensins (**e**).

cells[31] is of a similar order of magnitude as CTCF-defined loop domains (~180 kb)[33]. Supercoiled chromatin loop domains may stimulate intramolecular interactions such as enhancer–promoter interactions[34], or may act as efficient recruitment sites for topoisomerases by localizing topological stresses distributed along chromatin into defined regions. Indeed, various studies have reported a co-localization of topoisomerases and SMCs in both bacteria[35] and eukaryotes[9,10].

Our AFM data showed that yeast condensin with ATP can introduce DNA supercoiling into plasmid DNA. This is consistent with findings from previous in vitro gel-based and electron microscopy studies for condensin I complexes from frogs[11,12] and humans[14]. Together with our findings from imaging experiments, this indicates that supercoiled loop formation involves the active generation of supercoils in addition to the passive absorption of existing plectonemes. The supercoil-generating activity of condensin raises the question of its implications for mitotic chromosome condensation. SMC-induced generation of DNA supercoils naturally condenses DNA and may facilitate the decatenation of sister chromatids during the onset of anaphase[7,36].

In summary, our study provides mechanistic insight into the dynamic interplay between condensin-mediated loop extrusion and plectonemic DNA supercoils. We observed a rich phenomenology, including the topology-stimulated loading of condensin, the absorption of plectonemic DNA by extrusion of the supercoiled loop, and the active generation of DNA supercoils. These findings provide crucial insight into understanding loop extrusion of more complex DNA topologies, which is important, as supercoiling is one of the fundamental properties of cellular DNA that helps constitute higher levels of chromosome organization.

Online content

Any methods, additional references, Nature Research reporting summaries, source data, extended data, supplementary information, acknowledgements, peer review information; details of author contributions and competing interests; and statements of data and code availability are available at https://doi.org/10.1038/s41594-022-00802-x.

References

1. Yatskevich, S., Rhodes, J. & Nasmyth, K. Organization of chromosomal DNA by SMC complexes. *Annu. Rev. Genet.* **53**, 445–482 (2019).
2. Ganji, M. et al. Real-time imaging of DNA loop extrusion by condensin. *Science* **360**, 102–105 (2018).
3. Davidson, I. F. et al. DNA loop extrusion by human cohesin. *Science* **366**, 1338–1345 (2019).
4. Kim, Y., Shi, Z., Zhang, H., Finkelstein, I. J. & Yu, H. Human cohesin compacts DNA by loop extrusion. *Science* **366**, 1345–1349 (2019).
5. Golfier, S., Quail, T., Kimura, H. & Brugués, J. Cohesin and condensin extrude DNA loops in a cell-cycle dependent manner. *eLife* **9**, e53885 (2020).
6. Kim, E., Kerssemakers, J., Shaltiel, I. A., Haering, C. H. & Dekker, C. DNA-loop extruding condensin complexes can traverse one another. *Nature* **579**, 438–442 (2020).
7. Baxter, J. et al. Positive supercoiling of mitotic DNA drives decatenation by topoisomerase II in eukaryotes. *Science* **331**, 1328–1332 (2011).
8. Sutani, T. et al. Condensin targets and reduces unwound DNA structures associated with transcription in mitotic chromosome condensation. *Nat. Commun.* **6**, 7815 (2015).
9. Minchell, N. E., Keszthelyi, A. & Baxter, J. Cohesin causes replicative DNA damage by trapping DNA topological stress. *Mol. Cell* **78**, 739–751. e8 (2020).
10. Canela, A. et al. Genome organization drives chromosome fragility. *Cell* **170**, 507–521.e18 (2017).
11. Kimura, K. & Hirano, T. ATP-dependent positive supercoiling of DNA by 13S condensin: a biochemical implication for chromosome condensation. *Cell* **90**, 625–634 (1997).
12. Kimura, K., Rybenkov, V. V., Crisona, N. J., Hirano, T. & Cozzarelli, N. R. 13S condensin actively reconfigures DNA by introducing global positive writhe. *Cell* **98**, 239–248 (1999).
13. Bazett-Jones, D. P., Kimura, K. & Hirano, T. Efficient supercoiling of DNA by a single condensin complex as revealed by electron spectroscopic imaging. *Mol. Cell* **9**, 1183–1190 (2002).
14. Kimura, K., Cuvier, O. & Hirano, T. Chromosome condensation by a human condensin complex in *Xenopus* egg extracts. *J. Biol. Chem.* **276**, 5417–5420 (2001).
15. Eeftens, J. M. et al. Real-time detection of condensin-driven DNA compaction reveals a multistep binding mechanism. *EMBO J.* **36**, 3448–3457 (2017).
16. Gutierrez-Escribano, P. et al. Purified Smc5/6 complex exhibits DNA substrate recognition and compaction. *Mol. Cell* **80**, 1039–1054.e6 (2020).
17. Sun, M., Nishino, T. & Marko, J. F. The SMC1-SMC3 cohesin heterodimer structures DNA through supercoiling-dependent loop formation. *Nucleic Acids Res.* **41**, 6149–6160 (2013).
18. Ganji, M., Kim, S. H., van der Torre, J., Abbondanzieri, E. & Dekker, C. Intercalation-based single-molecule fluorescence assay to study DNA supercoil dynamics. *Nano Lett.* **16**, 4699–4707 (2016).
19. Kim, S. H. et al. DNA sequence encodes the position of DNA supercoils. *eLife* **7**, e36557 (2018).
20. van Loenhout, M. T. J., de Grunt, M. V. & Dekker, C. Dynamics of DNA supercoils. *Science* **338**, 94–97 (2012).
21. Ganji, M. et al. Real-time imaging of DNA loop extrusion by condensin. *Science* **360**, 102–105 (2018).
22. Thundat, T. et al. Atomic force microscopy of DNA on mica and chemically modified mica. *Scanning Microsc.* **6**, 2 (1992).
23. Balke, V. L. & Gralla, J. D. Changes in the linking number of supercoiled DNA accompany growth transitions in *Escherichia coli*. *J. Bacteriol.* **169**, 4499–4506 (1987).
24. Freeman, L., Aragon-Alcaide, L. & Strunnikov, A. The condensin complex governs chromosome condensation and mitotic transmission of rDNA. *J. Cell Biol.* **149**, 811–824 (2000).

25. Brandão, H. B. et al. RNA polymerases as moving barriers to condensin loop extrusion. *Proc. Natl Acad. Sci.* **116**, 20489–20499 (2019).

26. Johzuka, K., Terasawa, M., Ogawa, H., Ogawa, T. & Horiuchi, T. Condensin loaded onto the replication fork barrier site in the rRNA gene repeats during S phase in a *FOB1*-dependent fashion to prevent contraction of a long repetitive array in *Saccharomyces cerevisiae*. *Mol. Cell. Biol.* **26**, 2226–2236 (2006).

27. Jeppsson, K. et al. The chromosomal association of the Smc5/6 complex depends on cohesion and predicts the level of sister chromatid entanglement. *PLoS Genet.* **10**, e1004680 (2014).

28. Guo, M. S., Kawamura, R., Littlehale, M. L., Marko, J. F. & Laub, M. T. High-resolution, genome-wide mapping of positive supercoiling in chromosomes. *eLife* **10**, e67236 (2021).

29. Marko, J. F. & Neukirch, S. Competition between curls and plectonemes near the buckling transition of stretched supercoiled DNA. *Phys. Rev. E: Stat., Nonlinear, Soft Matter Phys.* **85**, 011908 (2012).

30. Racko, D., Benedetti, F., Dorier, J. & Stasiak, A. Transcription-induced supercoiling as the driving force of chromatin loop extrusion during formation of TADs in interphase chromosomes. *Nucleic Acids Res.* **46**, 1648–1660 (2018).

31. Naughton, C. et al. Transcription forms and remodels supercoiling domains unfolding large-scale chromatin structures. *Nat. Struct. Mol. Biol.* **20**, 387–395 (2013).

32. Achar, Y. J., Adhil, M., Choudhary, R., Gilbert, N. & Foiani, M. Negative supercoil at gene boundaries modulates gene topology. *Nature* **577**, 701–705 (2020).

33. Rao, S. S. P. et al. A 3D map of the human genome at kilobase resolution reveals principles of chromatin looping. *Cell* **159**, 1665–1680 (2014).

34. Benedetti, F., Dorier, J. & Stasiak, A. Effects of supercoiling on enhancer–promoter contacts. *Nucleic Acids Res.* **42**, 10425–10432 (2014).

35. Nolivos, S. et al. MatP regulates the coordinated action of topoisomerase IV and MukBEF in chromosome segregation. *Nat. Commun.* **7**, 10466 (2016).

36. Sen, N. et al. Physical proximity of sister chromatids promotes Top2-dependent intertwining. *Mol. Cell* **64**, 134–147 (2016).

Methods

Condensin holocomplex purification and fluorescent labeling. We used our previously published expression, purification and labeling procotols[2,6] to purify the pentameric *Saccharomyces cerevisiae* condensin complex.

Synthesis and purification of coilable 42-kb DNA construct. A coilable 42-kb DNA construct was made using linearized cosmid-I95[37], containing on either end a biotin–DNA handle with multiple biotins. The cosmid-I95 plasmid was amplified in a NEB 5 (New England Biolabs, C2987H), and the DNA was purified using a QIAfilter Plasmid Midi Kit (Qiagen, 12243). Biotin-containing handles were made using a PCR on pBluescript SK+ (Stratagene) with GoTaq G2 DNA polymerase (Promega, M7845), in the presence of 1/5 biotin-16-dUTP (Jena Bioscience, NU-803-BIO16-L) to dTTP (Thermo Fisher Scientific, 10520651). The PCR was done using primer CD21 (GACCGAGATAGGGTTGAGTG) and CD22 (CAGGGTCGGAACAGGAGAGC), resulting in a 1,238 base pair (bp) DNA fragment that contained multiple biotins. This was cleaned up using a PCR cleanup kit (Promega, A9282). The biotin handle and cosmid-I95 DNA were both digested for 2 h at 37 °C with SpeI-HF (New England Biolabs, R3133L) and subsequently heat-inactivated for 20 min at 80 °C, resulting in linear ~42-kb DNA and ~600-bp biotin handles. The digested products were mixed together, and we used a 10:1 molar access of the biotin handle to linear cosmid-I95. We then added T4 DNA ligase (New England Biolabs, M0202L) in the presence of 1 mM ATP overnight at 16 °C and subsequently heat-inactivated the next morning for 20 min at 65 °C. The resulting coilable 42-kb DNA construct was cleaned up using ÄKTA pure, with a homemade gel filtration column containing approximately 46 ml of Sephacryl S-1000 SF gel filtration media (Cytiva), run with TE + 150 mM NaCl₂ buffer. The sample was run at 0.2 ml min⁻¹, and we collected 0.5 ml fractions.

Single-molecule visualization assay for studying condensin-mediated loop extrusion on supercoiled DNA. For immobilization of the 42-kb coilable DNA, we introduced 50 μl of ~1 pM biotinylated DNA molecules at a flow rate of 2–3 μl min⁻¹. Then, we immediately flowed 100 μl of a washing buffer (40 mM Tris-HCl, pH 8.0, 20 mM NaCl, 0.4 mM EDTA) at the same flow rate to ensure stretching and tethering of the other end of the DNA to the surface. We typically obtained a stretch of around 20–40% of the DNA contour length.

To induce positive supercoiling of the tethered DNA, we flowed in 250 nM SxO in condensin buffer (40 mM Tris-HCl, pH 7.5, 50 mM NaCl, 2.5 mM MgCl₂, 1 mM dithiothreitol (DTT), 5% (w/v) D-dextrose, 2 mM Trolox, 40 μg ml⁻¹ glucose oxidase, 17 μg ml⁻¹ catalase) with 5 mM ATP. To prepare negatively supercoiled DNA, we first immobilized DNA to the surface in the presence of a high concentration of SxO (1 μM in condensin buffer with 5 mM ATP), and subsequently reduced the dye concentration to 250 nM for the measurements. The subsequent release of prebound SxO dyes after immobilization of the DNA results in negative supercoiling of the DNA.

Real-time observation of supercoiled-DNA loop extrusion by condensin was carried out by introducing condensin (1–2 nM) and ATP (5 mM) in the condensin buffer. Fluorescence imaging was achieved by using an objective-type total internal reflection fluorescence (TIRF) microscope. SxO-stained DNA and Atto 647N-labeled condensin were simultaneously imaged by alternating excitation of 532 nm and 640 nm lasers in HILO microscopy mode. All images were acquired with an EMCCD camera (iXon 897, Andor) with a frame rate of 10 Hz.

Data analysis for single-molecule imaging. Fluorescence images were recorded using custom-written LabVIEW 2011 software, and the obtained images were analyzed using custom-written Python 3.7 software. The noise from the images was removed using a machine-learning-based denoising method called 'Noise2Void' as published before[38]. Fluorescence-intensity kymographs were built from the intensity profiles of DNA and condensin molecules per time point. Each vertical line on the kymograph (for example, Fig. 1d) was obtained by summing fluorescence intensities of 11 pixels perpendicular to the DNA axis. Peaks on each vertical line from the kymograph were found using the peak-finding algorithm (scipy.signal.find_peaks) in SciPy[39], which finds all of the local maxima by comparing with the neighboring values. The plectonemic peaks were selected from the local maxima with a 20% threshold of the maximum peak prominences (relative peak intensities). This threshold removes the spurious low-intensity peaks.

Unlike non-loop-extruding condensins that bind and unbind at a fixed position on DNA, condensins bound on plectonemic supercoiled DNA (for example, Fig. 2a) diffuse along with the plectoneme[18,20]. To trace diffusing plectonemes and condensins, we consider peaks appearing in consecutive frames to be continuous if they appeared within 5 pixels (~375 nm or ~1 kb) of each other. To reduce false positives due to noise, we included only peaks that were observed for more than ten consecutive frames. Thus, individual diffusing plectonemes and plectoneme-bound condensins could be tracked over time.

The estimation of the co-localization probability of condensin and DNA plectoneme peaks (Fig. 2c) was performed as follows. From the tracked condensin and DNA peaks, we counted the peaks that had been in close proximity to each other (within 5 pixels, that is, ~375 nm or ~1 kb) for more than three consecutive

frames, and divided this by the total number of tracked condensin peaks. For the data analysis regarding Fig. 3a, we obtained the probability of finding a condensin peak per 1 kb of DNA length by summing the total number of detected condensin peaks over all time points, and dividing this by the DNA length (42 kb) and by measurement time. For the analysis regarding Fig. 2e,g, we determined the position of condensin along the buffer-flow-stretched plectoneme by detecting the two ends of plectoneme (that is, the stem and tip) per time point from the kymographs (for example, Fig. 2d) by fitting it with a super-Gaussian function. We then normalized the position of condensin peaks by the length of plectonemes at every time point. Note that as the condensin and DNA molecules were visualized at alternating time points that were 100 ms apart (alternative excitation mode), the normalized condensin position at every time point still can vary and result in a number larger than 1.

Sample preparation and data analysis for AFM imaging. For the preparation of the torsionally constrained DNA plasmid, pBlueScript SK+ (2,961 bp) DNA was purified from the NEB 5 at stationary phase using the QIAfilter Plasmid Midi Kit. To get constrained plasmid DNA without supercoils, we nicked the plasmid with nt.BspQI (New England Biolabs, R0644S) for 2 h at 60 °C, and heat-inactivated for 20 min at 80 °C. Some DNA was re-ligated overnight at 16 °C in the same buffer with T4 DNA ligase, in the presence of 1 mM ATP. Both the nicked and re-ligated plasmid DNA were subsequently purified using a PCR cleanup kit.

Condensin stock solution was first diluted to a concentration of 25 nM. Then, the condensin was diluted into a volume of 20 μl containing 0.5 nM DNA, 1–2 nM condensin in 50 mM Tris-HCl, pH 7.5 and 50 nM NaCl. The condensin–DNA solution was incubated for 5 min. Afterward, the solution was supplemented with MgCl₂ to a final concentration of 5 mM and deposited onto a freshly cleaved mica. After 30 s, the surface was thoroughly washed with 3 ml of Milli-Q water and dried under nitrogen airflow[40].

Images were taken with a MultiMode 2 AFM (Bruker) using ScanAsyst-Air-HR tips (Bruker). The AFM was operated using PeakForce Tapping mode for imaging in air, at room conditions. Image data and processing (plane subtraction and flattening) was done with Gwyddion software.

For the data analysis, we classified DNA molecules as 'entangled' if the molecules had one or more 'crossovers', or had local regions with a close and parallel proximity of both DNA helices (Fig. 5b). The fraction of entanglement within a DNA molecule (Fig. 5c) was estimated by measuring the length of the entangled region divided by the contour length of the DNA. Note that when we measured the height profiles of individual DNA molecules along the contour of the molecules (see Extended Data Fig. 8), the entangled regions of DNA showed a mean height above 1.75 nm with local peaks with heights of ≥2 nm, whereas the nonentangled region had a mean height of 1.25 nm. This indicates that these entangled regions contain overlaps of two dsDNA molecules, which is expected if DNAs are intertwined.

Statistics and reproducibility. Data are presented as mean ± s.d. Statistical analyses were performed using two-sided *t*-tests. Details on individual statistical tests and the number of times individual experiments were replicated are noted in the respective figure legends. No statistical method was used to predetermine sample size. Experiments were not randomized, and investigators were not blinded to allocation during experiments and outcome assessment. Occasionally, data from fluorescent-labeled condensin imaging were excluded when the tracking of single molecules was not possible because of high background coming from nonspecific sticking of the protein to the surface (which was dependent on the surface quality of the flow cell). In these cases, the entire experiment was repeated.

Reporting summary. Further information on research design is available in the Nature Research Reporting Summary linked to this article.

Data availability

Source data files are available for Figs. 1e,g,h; 2c,e; 3g; 4a,b; 5b–d and 6g,h and Extended Data Figs. 1; 3b; 4a,b; 5c and 10a,b. Original imaging data are available upon request. Source data are provided with this paper.

Code availability

The Python-based data analysis source code used for the analysis of the imaging data is available at https://github.com/biswajitSM/LEADS.

References

37. Japaridze, A. et al. Hyperplectonemes: a higher order compact and dynamic DNA self-organization. *Nano Lett.* **17**, 1938–1948 (2017).
38. Krull, A., Buchholz, T.-O. & Jug, F. Noise2Void—learning denoising from single noisy images. In *Proc. IEEE/CVF Conf. Comput. Vis. Pattern Recognit.* 2124–2132 (IEEE, 2019).
39. Virtanen, P. et al. SciPy 1.0: fundamental algorithms for scientific computing in Python. *Nat. Methods* **17**, 261–272 (2020).
40. Lyubchenko, Y. L. & Shlyakhtenko, L. S. AFM for analysis of structure and dynamics of DNA and protein–DNA complexes. *Methods* **47**, 206–213 (2009).

Author contributions

E.K. and C.D. designed the single-molecule imaging experiments, E.K. performed the imaging experiments and analyzed the imaging data, A.M.G. performed the AFM experiments and analyzed the AFM data, B.P. contributed in image analyses, J.v.d.T. prepared the DNA construct, C.D. supervised the work, and all authors wrote the manuscript.

Competing interests

All authors declare that they have no competing interests.

Additional information

Extended data is available for this paper at https://doi.org/10.1038/s41594-022-00802-x.

Supplementary information The online version contains supplementary material available at https://doi.org/10.1038/s41594-022-00802-x.

Correspondence and requests for materials should be addressed to Cees Dekker.

Peer review information *Nature Structural and Molecular Biology* thanks Alice Pyne, Anders Hansen, and Jan Lipfert for their contribution to the peer review of this work. Primary Handling Editor: Carolina Perdigoto, in collaboration with the *Nature Structural and Molecular Biology* team. Peer reviewer reports are available.

**Reprints and permissions information** is available at www.nature.com/reprints.
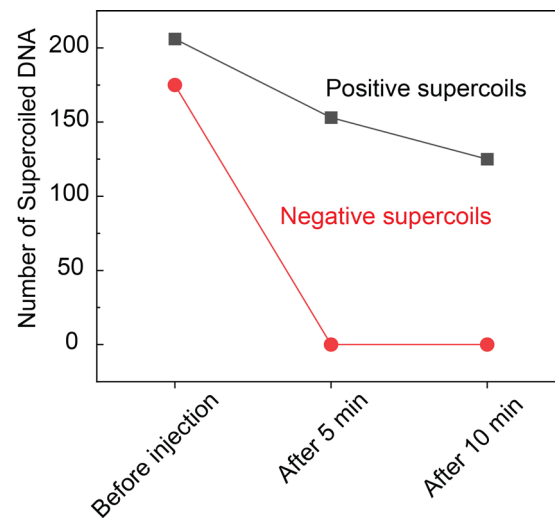
Extended Data Fig. 1 | Validation of our supercoiling generation assay. To confirm the handedness of supercoiling, we introduced Topoisomerase I from E. coli, which only relaxes negative supercoils, to our DNA molecules on the surface that were generated to have positive/negative supercoils via SxO intercalation reaction. For negative supercoils, all the DNA molecules relaxed within 5 minutes of incubation with Topo1, while in the case of positive supercoils, the amount of supercoiled molecules only decreased by 25. Since, independent of Topo1, DNA molecules can be also nicked by exposure of excitation laser (which would resolve the supercoiling), the actual fraction of positive supercoiled DNA in our assay should be well above 75%. These data confirm the handedness of the supercoiling generated via SxO intercalation.
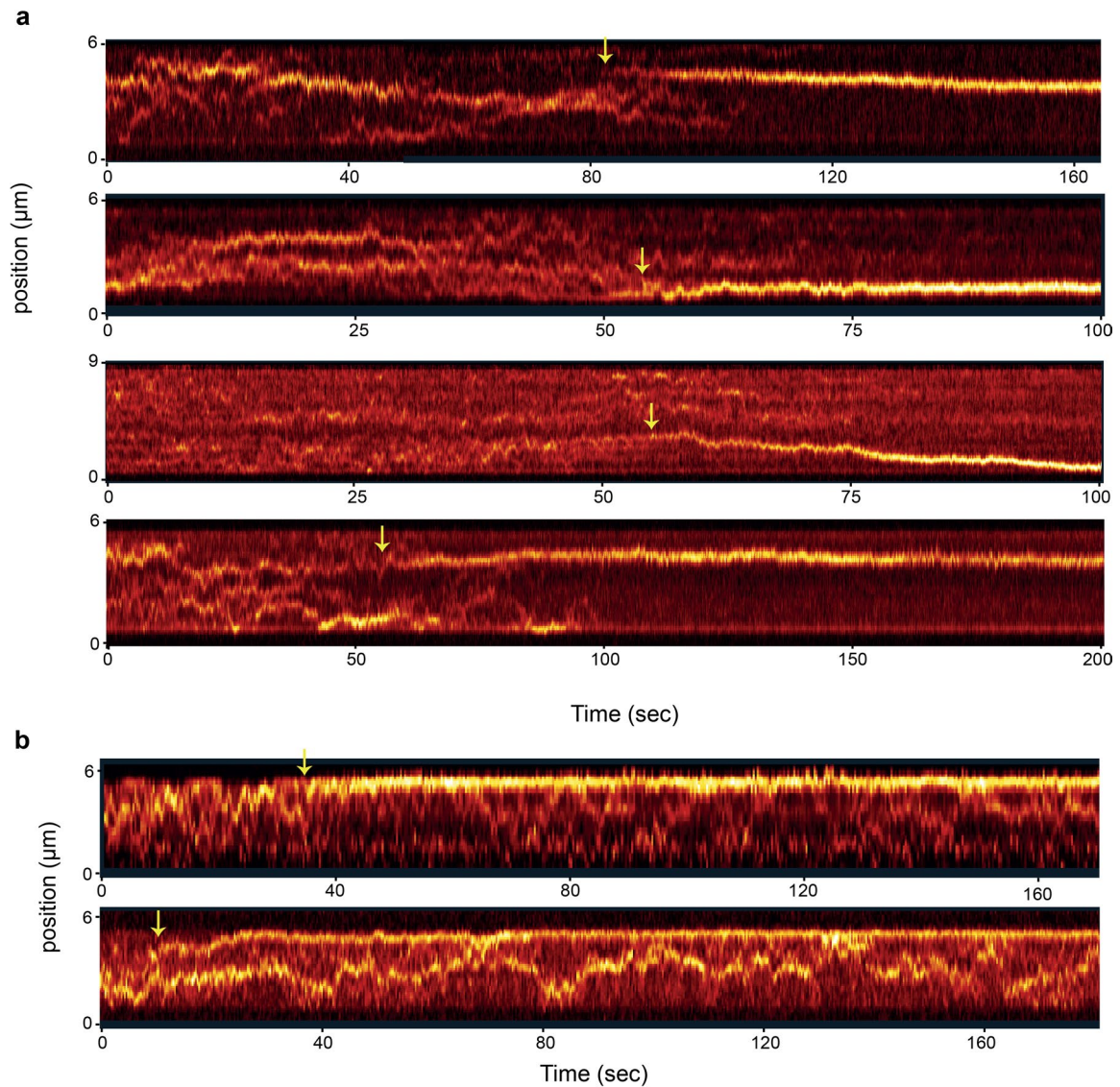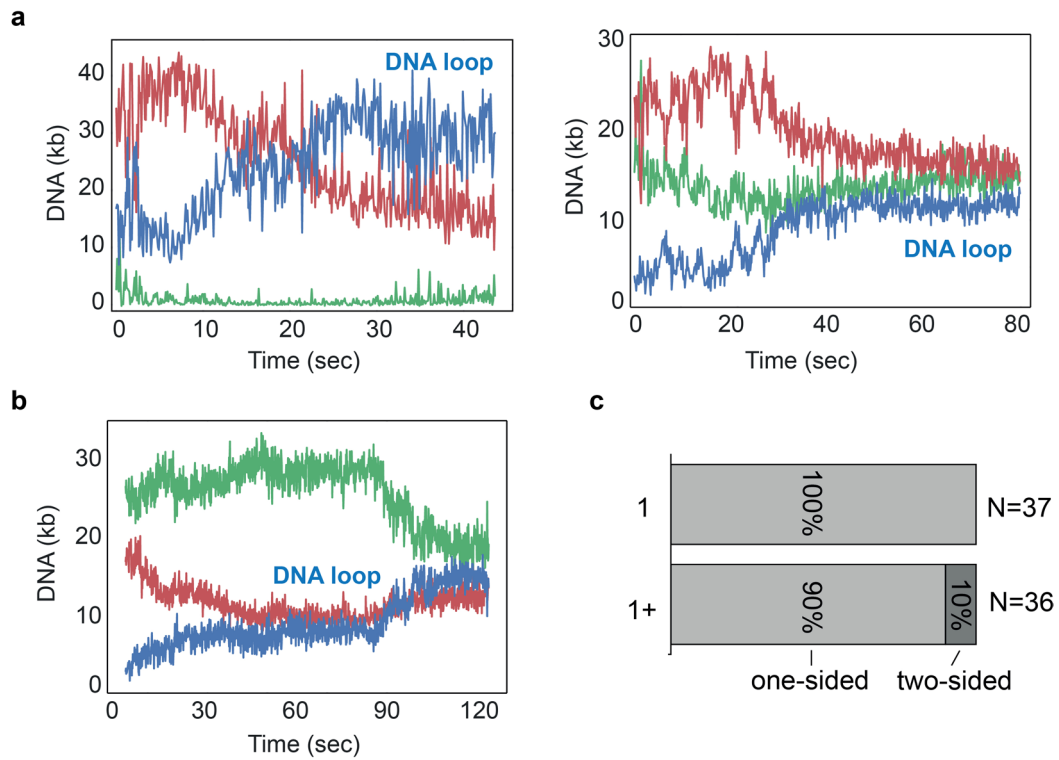
Extended Data Fig. 2 | Fluorescence-intensity kymographs showing additional examples of loop extrusion events on supercoiled DNA. (a) Examples showing condensin collects all the plectonemes upon loop extrusion and stabilizes them at its location. Yellow arrows show the location of the start of the gradually growing peak during loop extrusion. (b) Examples showing cases where condensin loop extrusion did not lead to absorption of all the plectonemes. In these events (11% of the total cases, Ntot=36), condensin was bound relatively close to the tethered end of DNA and the DNA loop extrusion was limited by reaching the end position of the DNA. Yellow arrows show the location of the start of the growing DNA loop.

a

b
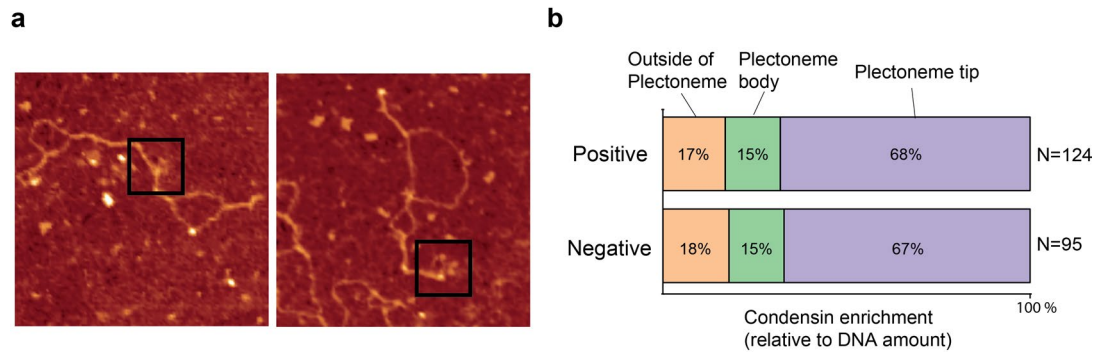
Extended Data Fig. 3 | Estimation of condensin-binding position on supercoiled DNA measured with AFM. a) Representative AFM images showing condensin binding near a plectoneme body (left) and near the plectoneme tip (right). Data represent 4 independent experiments. b) Statistics showing enrichment of condensin as observed outside of plectoneme, at plectoneme body, and at apical loops. In order to avoid possible supercoiling induced by condensin, the plasmids were incubated with AMP-PNP.
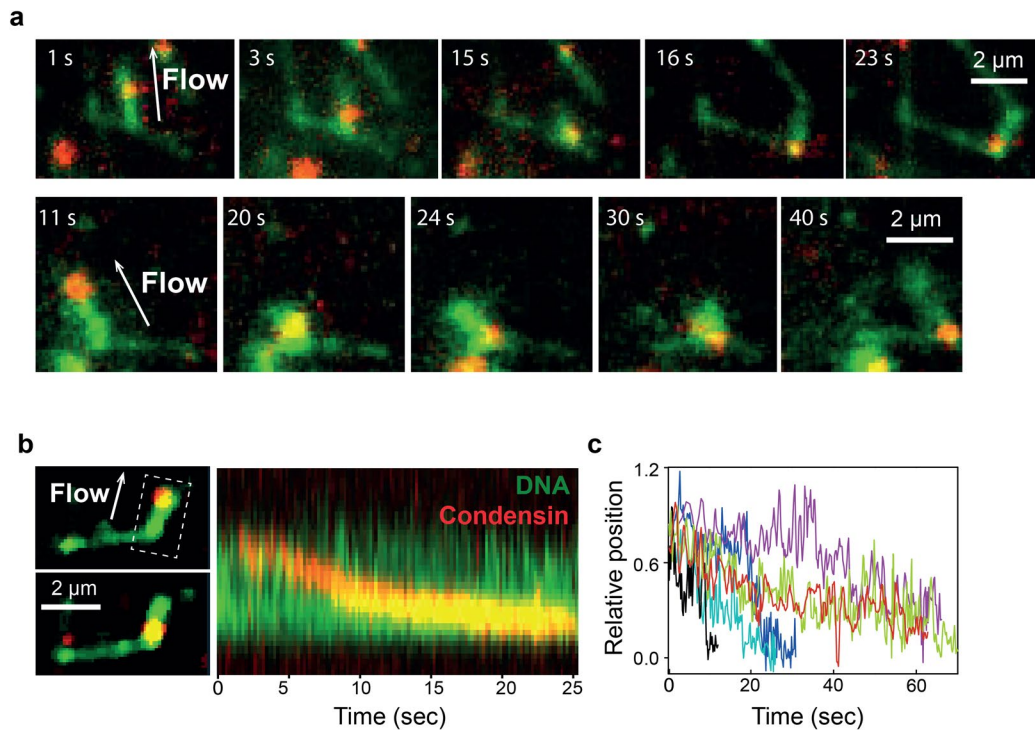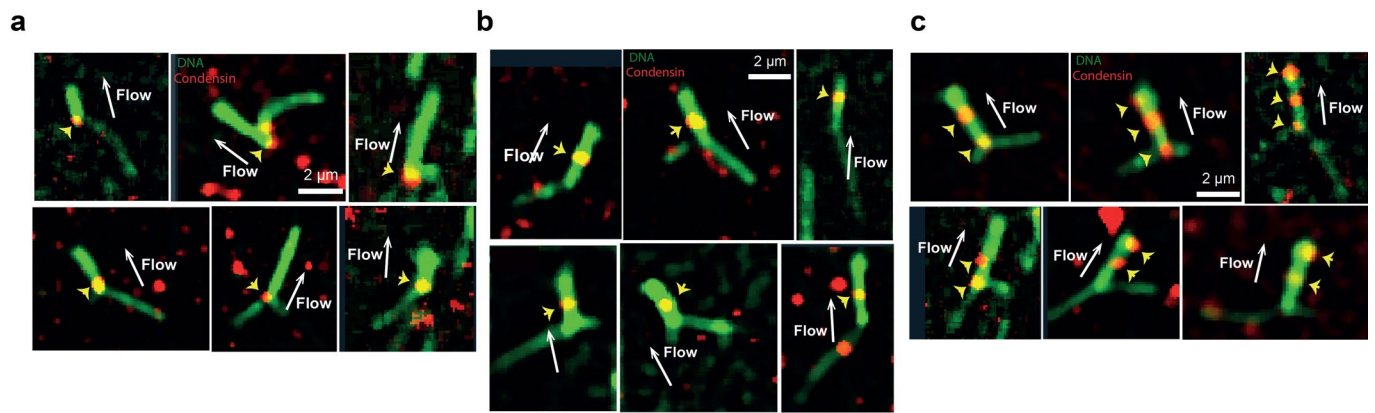
Extended Data Fig. 4 | Additional examples showing that condensin initially loads near a plectoneme tip and moves downwards during plectoneme loop extrusion. a) Snapshots showing condensin moving from the plectoneme tip (1st) towards the stem (till 3rd snapshot). Simultaneously the plectoneme becomes compacted and moves together with the condensin during extrusion while it grows back its length at later times (3rd – 5th frame). Data represent 3 independent experiments. b) Snapshot (left) and kymograph (right) showing condensin moving from the plectoneme tip towards the stem. Data represent 3 independent experiments. (c) Change in position for condensins that bound at the tip and moved along the length of DNA plectonemes extracted from the kymographs as in panel b for N = 6 molecules. The red colored trace corresponds to the kymograph in panel b.

Extended Data Fig. 5 | Condensin-mediated loop extrusion on supercoiled DNA is strictly asymmetric. (a) Examples of the DNA length calculated from the integrated fluorescence intensity kymographs of DNA loop extrusion by a single condensin on supercoiled DNA, showing asymmetric loop extrusion. (b) Same for an event where multiple condensins underlie the DNA loop, showing symmetric loop extrusion. (c) Statistics showing the ratios of the asymmetric and symmetric loop extrusion events observed for a single condensin (1) and multiple condensins (1+).
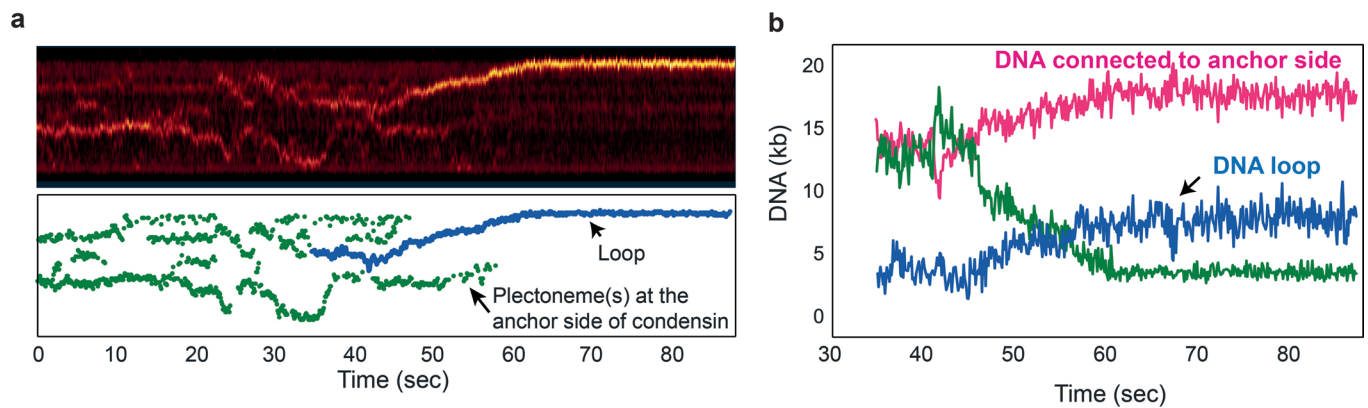
Extended Data Fig. 6 | While plectonemes connected to the anchor side of condensin disappear, the corresponding DNA amount does not decrease.
(a) Example kymograph (top) and the DNA peaks (bottom) detected during condensin-mediated loop extrusion on supercoiled DNA. (b) Corresponding DNA lengths calculated from the kymograph. During the loop growth (blue; 45 s- 60 s) the length of DNA connected to the anchor side of condensin (pink) did not decrease, but instead DNA was accumulated from the motor side of condensin (green). This indicates that the disappearance of plectoneme at the anchor side is not due to the absorbance of plectoneme into the loop but rather to the stretching of the DNA.

Extended Data Fig. 7 | Additional examples of condensin location along the plectoneme. Condensin was found to be located at (a) the stem or (b) the middle after extrusion of a supercoiled loop in the case of single condensin. (c) Additional examples where multiple condensins are located along the supercoiled loop. Data in (a-c) represent 5 independent experiments.
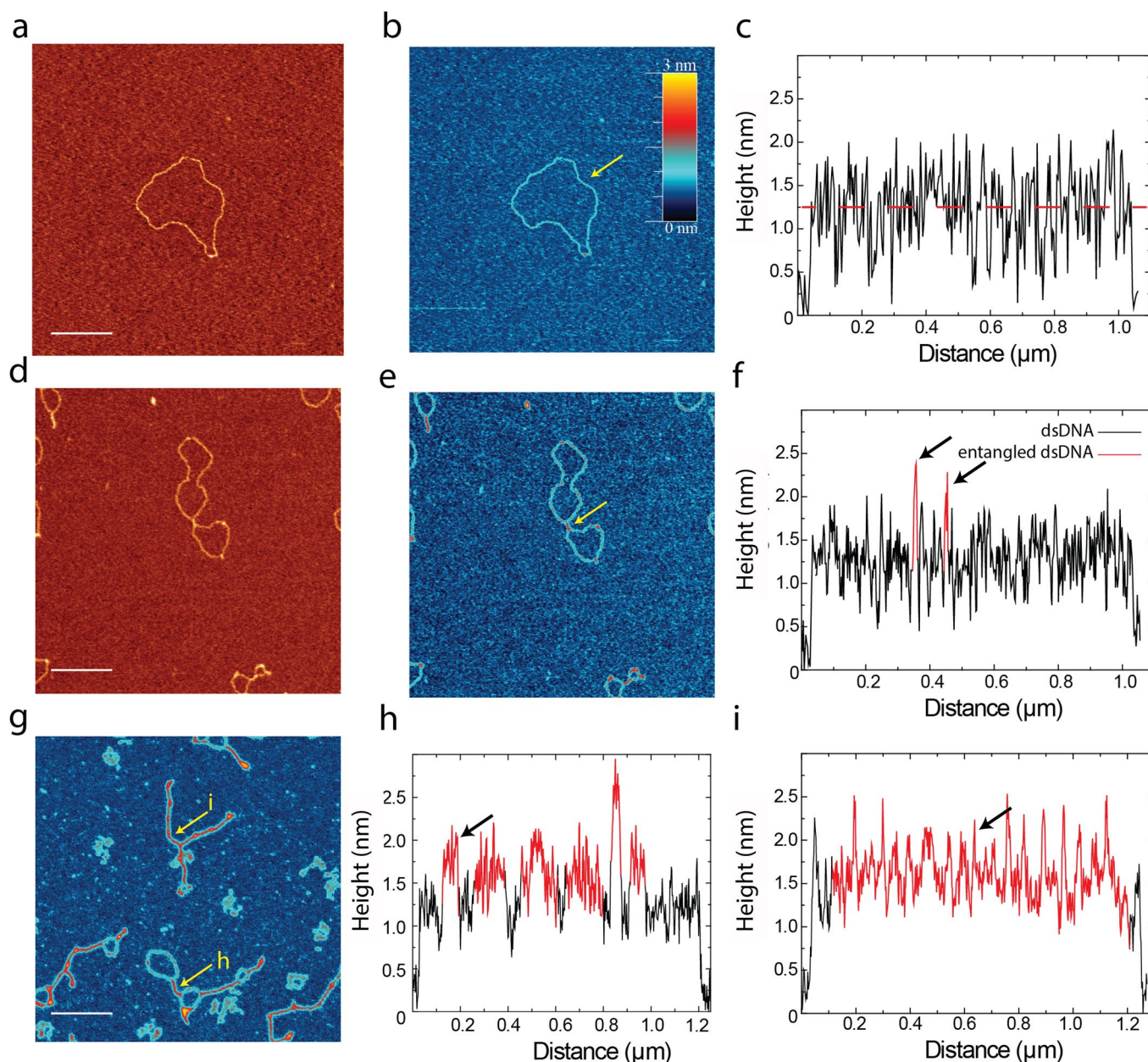
Extended Data Fig. 8 | AFM analysis of supercoiled DNA molecules. (a) AFM image of a non-entangled dsDNA molecule. (b) Same image in an expanded blue-red color scale to highlight the entangled regions of dsDNA (red) versus the non-entangled regions (light blue) and the mica (dark blue). Inset shows the Z color scale. Data in (a,b) represent 3 independent experiments. (c) Height profile along the molecule in a/b, showing an average height of 1.25 nm. (d) AFM image of a dsDNA molecule with one crossover. (e) Same image in an expanded blue-red color scale. The crossover point is denoted with a yellow arrow. Data in (d,e) represent 5 independent experiments. (f) Height profile along the molecule shown on d/e. A locally increased height of > 2 nm is observed at the crossing point (arrows). The arrows denote the two peaks that correspond to the crossing point – which is encountered twice upon tracking the contour of the DNA along this 'figure-8' profile. (g) AFM image of entangled dsDNA molecules. Yellow arrows signal the molecules of which the profiles are shown in panels h and i. Data represent 3 independent experiments. (h) Height profile along a molecule where the entangled patches are denoted in red. (i) Same for the molecule indicated by i in panel g. Notably, this molecule was almost entirely entangled along its full contour length. Scale bars are 200 nm.
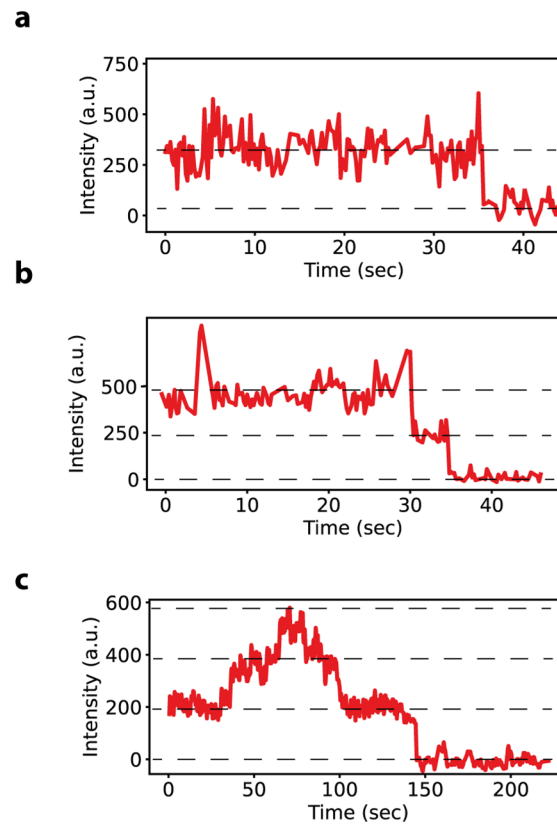
Extended Data Fig. 9 | Examples of bleaching time traces of fluorescence intensities of individual ATTO647N-labelled condensin complexes at the location of supercoiled loops. (a) Bleaching occurred in a single step-wise manner for condensin after a loop extrusion event. (b) Bleaching occurred in a double step-wise manner after an event where two condensins had merged into a single supercoiled DNA loop. (c) Bleaching occurred in a single step-wise manner for condensin after a loop extrusion event. Additional short binding events occurred at the plectoneme loop.
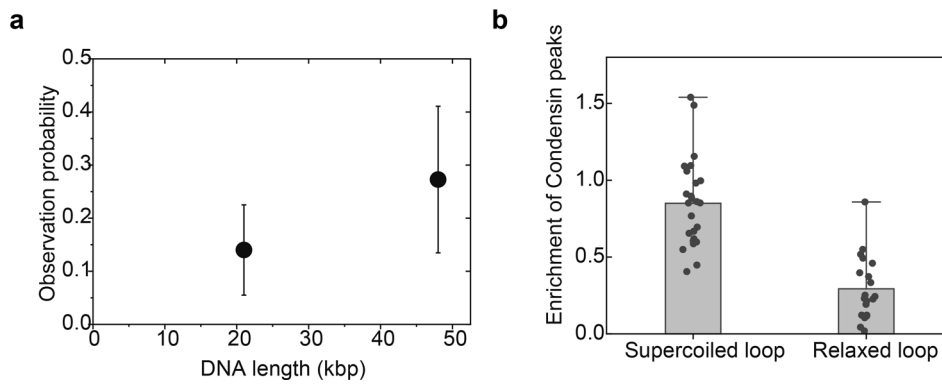
Extended Data Fig. 10 | Condensin binding is length and supercoiling dependent. (a) Observation probability of condensin on nicked DNA with two different lengths (21 kb and 48.5 kb), estimated by summing the total number of detected condensin peaks over all time points, and dividing this by the DNA length and measurement time. N = 8 molecules for 21 kb, N = 22 molecules for 48 kb length, respectively. (b) Condensin enrichment on supercoiled loops and relaxed loops, estimated by summing up the total intensity of the detected condensin peaks within the loop region with similar lengths (~60 % of its contour length). N = 25 molecules for supercoiled loops and N = 20 for relaxed loops, respectively. Data represent mean ± standard deviation.

Corresponding author(s): Cees Dekker

Last updated by author(s): Mar 24, 2022

Reporting Summary

Nature Research wishes to improve the reproducibility of the work that we publish. This form provides structure for consistency and transparency in reporting. For further information on Nature Research policies, see our Editorial Policies and the Editorial Policy Checklist.

Statistics

For all statistical analyses, confirm that the following items are present in the figure legend, table legend, main text, or Methods section.

n/a	Confirmed	
☐	☒	The exact sample size (*n*) for each experimental group/condition, given as a discrete number and unit of measurement
☐	☒	A statement on whether measurements were taken from distinct samples or whether the same sample was measured repeatedly
☐	☒	The statistical test(s) used AND whether they are one- or two-sided *Only common tests should be described solely by name; describe more complex techniques in the Methods section.*
☒	☐	A description of all covariates tested
☒	☐	A description of any assumptions or corrections, such as tests of normality and adjustment for multiple comparisons
☐	☒	A full description of the statistical parameters including central tendency (e.g. means) or other basic estimates (e.g. regression coefficient) AND variation (e.g. standard deviation) or associated estimates of uncertainty (e.g. confidence intervals)
☐	☒	For null hypothesis testing, the test statistic (e.g. *F*, *t*, *r*) with confidence intervals, effect sizes, degrees of freedom and *P* value noted *Give P values as exact values whenever suitable.*
☒	☐	For Bayesian analysis, information on the choice of priors and Markov chain Monte Carlo settings
☒	☐	For hierarchical and complex designs, identification of the appropriate level for tests and full reporting of outcomes
☒	☐	Estimates of effect sizes (e.g. Cohen's *d*, Pearson's *r*), indicating how they were calculated

Our web collection on statistics for biologists contains articles on many of the points above.

Software and code

Policy information about availability of computer code

Data collection	The fluorescence imaging data used in this study were collected via custom-written Labview 2011 software.
Data analysis	The fluorescence images were analysed using custom-written Python 3.7 software. The AFM image data were processed (plane subtraction and flattening) with Gwyddion 2.60 software.

For manuscripts utilizing custom algorithms or software that are central to the research but not yet described in published literature, software must be made available to editors and reviewers. We strongly encourage code deposition in a community repository (e.g. GitHub). See the Nature Research guidelines for submitting code & software for further information.

Data

Policy information about availability of data

All manuscripts must include a data availability statement. This statement should provide the following information, where applicable:
- Accession codes, unique identifiers, or web links for publicly available datasets
- A list of figures that have associated raw data
- A description of any restrictions on data availability

The Python code used in this study will be available via a link to GitHub (https://github.com/biswajitSM/LEADS) after the manuscript regarding this analysis program is published. The statistical data files for this study are available in source data file. The original imaging data are available from the corresponding author upon reasonable request due to the large size of data.

Field-specific reporting

Please select the one below that is the best fit for your research. If you are not sure, read the appropriate sections before making your selection.

☒ Life sciences   ☐ Behavioural & social sciences   ☐ Ecological, evolutionary & environmental sciences

For a reference copy of the document with all sections, see nature.com/documents/nr-reporting-summary-flat.pdf

Life sciences study design

All studies must disclose on these points even when the disclosure is negative.

Sample size	No statistical method was used to determine sample size. Sample size was chosen based on our previous publications on similar topics (see e.g. DOI: 10.1126/science.aar7831, https://doi.org/10.1038/s41586-020-2067-5, https://doi.org/10.7554/eLife.36557.001). The precise number for sample size supporting respective findings are stated in the manuscript.
Data exclusions	Some of the data were excluded due to poor imaging quality that is insufficient for the further analysis.
Replication	All results in the paper are drawn from the analysis of multiple independent experiments (11 independent experiments for non-labeled proteins and 8 independent experiments for fluorescent-labeled proteins)and all the findings were highly reproducible. The data regarding fluorescent-labeled condensin imaging, in some cases (2 out of 8 experiments), were not reproducible due to high background coming from non-specific sticking of protein to the surface, that is dependent on the surface quality of the flow cell. On such occasion, the entire experiment was discarded and repeated.
Randomization	Randomization is not relevant since our study investigates the interactions between two known biomolecules (condensin and supercoiled DNA).
Blinding	Blinding is not relevant to this work since our study investigates single-molecule interactions of a specific molecules of condensin and DNA supercoils.

Reporting for specific materials, systems and methods

We require information from authors about some types of materials, experimental systems and methods used in many studies. Here, indicate whether each material, system or method listed is relevant to your study. If you are not sure if a list item applies to your research, read the appropriate section before selecting a response.

Materials & experimental systems

n/a	Involved in the study
☒	☐ Antibodies
☒	☐ Eukaryotic cell lines
☒	☐ Palaeontology and archaeology
☒	☐ Animals and other organisms
☒	☐ Human research participants
☒	☐ Clinical data
☒	☐ Dual use research of concern

Methods

n/a	Involved in the study
☒	☐ ChIP-seq
☒	☐ Flow cytometry
☒	☐ MRI-based neuroimaging